\$ SUPER

Contents lists available at ScienceDirect

Spectrochimica Acta Part B: Atomic Spectroscopy

journal homepage: www.elsevier.com/locate/sab





Following laser-induced plasma stoichiometry with atomic absorption spectroscopy

Jonathan Merten *, Erin Nicholas, Shawnda Ethridge, Hannah Bariola, Shealyn Chestnut, Anna Anders, Jackie Brees, Mary Foster

Department of Chemistry and Physics, Arkansas State University, United States of America

ARTICLE INFO

Keywords: LA-AAS Plasma absorption spectroscopy Plasma chemistry Oxidation Laser ablation LIBS

ABSTRACT

Atomic absorption spectroscopy was used to measure the absolute vanadium and titanium masses present as neutral atoms in the plume formed by laser ablation of a titanium alloy sample. At delays between two and twenty microseconds, the absolute masses and temperatures were measured with time-resolved Boltzmann plots under pure helium and an 80:20 He/O₂ mixture. The Boltzmann plots, which include the ground term (in contrast to emission-based measurements), produced high-quality estimates of the plasma composition. Under helium, the metal vapors persisted beyond the longest \sim 20 μ s delays measured. The V:Ti stoichiometry was approximately as expected from the nominal sample composition at all times under He. However, under He:O₂, the atomic vapor disappeared entirely in under 10 μ s and the stoichiometry became more enriched in vanadium at increasing delays. This enrichment is interpreted in terms of the difference in first oxide bond energies of the two metals. There was evidence of loss of metal even under helium within the investigated 20 μ s window.

1. Introduction

Laser ablation is used for material processing, including superconductor and nanoparticle syntheses, as well as materials analysis (e.g. laser-induced breakdown spectroscopy, LIBS, and laser-ablation inductively coupled plasma mass spectrometry, LA-ICPMS). [1–5] Because the laser-induced plasma (LIP) is most often studied by thermal emission spectroscopy, data typically represent the earlier, hotter, and therefore more thermally emissive times in the plasma's evolution- the first few microseconds (see References [6, 7] for extensive discussion of plasma diagnostics techniques relevant to the LIP). Otherwise, static information about the ablation process is available by sampling particles formed by various processes (spallation, splashing, condensation, aggregation, etc.) or by examining the crater left by the ablation. Crater measurements give little insight into the dynamic processes (e.g. condensation, evaporation, chemical reactions) occurring in the plasma after the initial material removal, unfortunately, and particle sampling and analysis are both complex.

Recently, several groups have returned to absorption spectroscopy to characterize the fast-evolving LIP dynamically at these later times where linewidths are narrowed and the atomic state distribution function (ASDF) has collapsed to lower-lying levels. [8] Because absorption and

emission measurements in the plasma may probe different populations and therefore, regions of the inhomogeneous plasma, they provide distinct and complementary views of the LIP phenomenon. [9] In addition to providing insight into the relative atomic state distribution function inclusive of the ground state, absorption spectroscopy allows measurement of absolute quantities of atomized material in the plasma to the extent that oscillator strengths are known. [10]

The plasma atmosphere is known to have substantial impact on LIP formation and evolution because of differences in cover gas ionization energy, density, thermal conductivity and chemical reactivity. [11–14] From an applications standpoint, the impact of cover gas on spectral profiles is important to implementing laser-ablation atomic absorption spectroscopy as a technique for measuring isotope ratios. [15] Additionally, the effect of ambient oxygen on plasma evolution is interesting in light of its implications for the LIBS or LA-analytical plasma's chemical representation of the sample or even for the plasma's potential as a practical simulant for nuclear explosions. [16–22] This chemistry may be somewhat unavoidable as some studies have found that even trace levels of oxygen in otherwise inert atmospheres are sufficient for measurable oxide formation in the LIP. [23] Irrespective of the atmosphere, such molecule formation in plasma is typically studied with *emission* spectroscopy. Unfortunately, as De Giacomo and Hermann

E-mail address: jmerten@astate.edu (J. Merten).

 $^{^{\}ast}$ Corresponding author.

point out, molecular thermal emission measurements are only feasible as a diagnostic with the subset of diatomic species that simultaneously possess moderate bond strengths and low electronic excitation energies such that bonds can form in a plasma that is still hot enough to populate the excited molecular states necessary for observation of thermal rovibronic emission spectra. [24]

In the present study, we use atomic absorption spectroscopy to measure the titanium and vanadium stoichiometry of a LIP formed under inert and reactive atmospheres. While there have been studies of plasma stoichiometry by laser-ablation atomic-absorption spectroscopy in the past [25], to our knowledge, ours is the first one to measure the entire plasma's composition rather than a single line of sight. Given the expected inhomogeneity of the plasma, such whole-plasma absorption measurements should allow important insight into the chemical and physical processes occurring as the plasma cools and the neutral atomic mass disappears. Ideally, these measurements can complement theoretical studies. [20,22]

2. Experimental

A commercial sample of titanium 10–2-3 (nominal alloy composition 85% titanium, 10% vanadium, 2% iron and 3% aluminum by mass) was ablated under 300 mbar of either UHP He or a commercially available 80/20 (by volume) mixture of He and O_2 . The chamber was pumped down and flushed with the appropriate gas four times, then held with a static atmosphere for the duration of a measurement at a given plasma mapping (~2000 laser shots). The chamber was opened and the windows and ablation-laser-focusing lens (located inside the chamber) cleaned after each ~2000-shot campaign. Ablation was with a Big Sky Ultra (Nd:YAG) operated at 1064 nm and focused through a $\rm f=10~cm$ best form lens placed at 9.5 cm. The ablation laser energy was reduced to 19 mJ with a half waveplate and a polarizing beamsplitter. The beam was also expanded slightly to protect chamber windows and to increase the effective numerical aperture of the focusing optic.

The plasma was probed with a "pseudocontinuum" pulse generated by an optical parametric oscillator (OPO, Ekspla 342A, Vilnius). The delay of the probe pulse relative to the ablation event was controlled with a DG 645 delay generator (Stanford Instruments). The OPO energy was attenuated with an achromatic half waveplate (Thorlabs) and a polarizing beamsplitter before spatial filtering. The spatially filtered beam was expanded and focused into the plasma at a high F/# to generate a beam waist of ~250 µm and a Rayleigh length much longer than the plasma dimensions. The probe pulse was separated into probe and reference arms by a plate beamsplitter before the sample chamber, allowing a dual-beam-in-space measurement paradigm. The probe beam was collected with an achromatic lens after the plasma and focused into a large-mode-area single-mode photonic crystal fiber. The reference beam was similarly directed into its own fiber. The fibers' outputs were collimated with achromats and the beams were recombined with a second beamsplitter, leaving a slight relative angular divergence. The nearly parallel beams were focused into the spectrometer with a common lens in such a manner as to produce two separate spots at the spectrograph's entrance slit, with spatially separated spectra produced at the detector.

The probe and reference beams were dispersed with a custom echelle spectrometer (ELIAS I, LTB Lasertechnik Berlin) modified by the manufacturer to allow simultaneous measurement of probe and reference arms on a single ICCD (usb iStar, Andor, Belfast). It was not feasible to measure the order-dependent resolving power at each wavelength, but $R\sim5\times10^5$ is a reasonable estimate when the grating was operated in single pass. The spectrograph is capable of double-pass measurements, but the resulting decrease in throughput combined with an increase in scatter (i.e. stray light) recommends against double-pass absorption measurements when possible. Although resolving power was not measured, the dispersion at each wavelength position was determined by inserting a 6.29 mm fused silica etalon in the probe beam path

and observing its modulation of the pseudocontinuum probe spectrum. During acquisition, the probe energy was kept below the level producing noticeable bleaching of the transition.

Absorption spectra were calculated for each probe/reference pair as log₁₀ using custom Labview routines that include an empirical alignment of the probe and reference spectra. In the event of high absorbance $(\log_{10}(I_0/I) > 1.3)$, the measurements were made dual-beam-in-time (i. e. sequentially with the reference beam blocked) to prevent loss of linearity due to crosstalk between probe and reference spectra in a given ICCD frame. For dual-beam-in-space measurements, 45 simultaneous spectral pairs (one probe, one reference) were collected at each plasma location. Of the 45, fifteen probed a plasma and 30 served as "blank" measurements with the triggering of the Q-switch of the ablation laser inhibited at the delay generator. The acquisition of sample and blank measurements was alternated using a homemade digital logic circuit that permitted Q-switching only when appropriate. Each 45-spectrum sequence was preceded by 5 sample-prep shots (i.e. "cleaning shots"). The sample was rotated to present a fresh surface after each 5+15ablation sequence.

Peaks were fit to a Voigt model using Origin 9.2 (Originlab, Northampton, MA) when SNR was adequate. In order to avoid overfitting, a simple Doppler model was used for low-SNR data. Because the combination of hyperfine and isotope shifts for the titanium lines was less than the measured linewidths, these were well-fit by the Voigt model. The substantial hyperfine structure of the vanadium (nuclear spin = 7/2) lines meant that there was some slight error in neglecting hyperfine structure when fitting the spectrum. In order to minimize this error, vanadium transitions with (relatively) less hyperfine splitting were selected.

The mass in a given lower level (m_l) was calculated from the sum of peak areas measured in building the plasma line-of-sight map according to: [10].

$$\frac{ln(10) \bullet M \bullet \Delta x \bullet \Delta y \bullet \int abs(\lambda)d\lambda}{N_A \bullet \lambda^2 \bullet \int_{lu} \bullet 8.8 \times 10^{-15}} = mass_l$$
 (1)

where M is the molar mass, Δx and Δy are the measurement spacings in the imaging grid, N_A is Avogadro's constant, λ is the transition wavelength, and f_{lu} is the transition oscillator strength. The constant in the denominator is evaluated in units of meters. Strictly speaking, absorption is proportional to the difference in the degeneracy-normalized upper and lower level occupancies. Eq. (1) neglects any substantial population of the upper level of a transition, a reasonable assumption for the transitions used here since probe photon energies exceed 16,000 cm $^{-1}$. Transition data were taken from the NIST atomic spectral database and are summarized in Table 1.

Table 1- details of transitions used. See Reference [26].

Element	Lower term symbol	g	E _{lower} (cm ⁻¹)	f (unitless)	Wavelength (nm)
				7.91 ×	
Ti	$^{3}F_{3}$	7	170	10^{-4}	521.970
				$2.01 \times$	
Ti	$^{3}F_{4}$	9	386	10^{-4}	546.050
				4.57 ×	
Ti	$^{3}F_{4}$	9	386	10^{-4}	525.210
	_			2.33 ×	
Ti	⁵ F ₃	7	6661	10^{-3}	504.061
	2			1.30 ×	
Ti	³ F ₄	9	11,776	10^{-2}	549.015
	4			7.90 ×	100.010
V	$^{4}F_{3/2}$	4	0	10 ⁻³	483.242
**	6rs		0011	2.45 ×	440 700
V	$^{6}D_{7/2}$	8	2311	10^{-2}	443.783
V	$^{4}D_{7/2}$	8	8715	1.07×10^{-1}	609.021
v	$\nu_{7/2}$	0	0/13	10	007.021

The degeneracy-normalized *absolute masses* in a series of levels (each summed over the whole plasma) were used to generate linearized Boltzmann plots, with temperatures extracted in the usual way. Because absorption measurements can give absolute masses, the total atomized mass of each element (neglecting ions) in the plasma was calculated from the Boltzmann plots as:

$$mass_t = Q(T) \bullet e^b \tag{2}$$

where Q(T) is the temperature-dependent electronic partition function and is taken from the NIST website or calculated from data therein and b is the y-intercept of the Boltzmann plot.

3. Results and discussion

The line-of-sight maps of ground term absorption are given in Fig. 1. Note that each map is individually scaled to emphasize morphology rather than the relative quantity in a given plasma at a given time. Under both gases, the earliest data point (2 µs) shows a hollow morphology with a particular "cap" of material distal to the sample surface. The extent and nature of the material in the central void is unclear and will be the topic of a future study designed to give access to ionized states in addition to the neutrals measured here. The void could be expected to result from turbulent mixing as gas rushes in from the base of the plasma, for example as modeled by Gornushkin et al. [22] The present data do not show any evidence of the expected mushroom cloud "stem," perhaps because this feature has already dissipated through mixing by the first time measured. It is interesting to note that these plasmas do not show the high concentration of absorbing atoms close to the sample surface observed with our previous measurements. [10] Those previous data were collected at a higher pressure of helium and with a larger laser spot size and higher ablation pulse energy, presumably resulting in different fluid dynamics.

In the present data, the plasmas under pure He reach their maximum spatial extent by $3.5~\mu s$ and are morphologically stable out to 11~u s, with the main change being a slow narrowing after $3.5~\mu s$. The plasmas under HeO (as defined by the spatial extent of the ground-state Ti atoms) are smaller at all of the times measured here and shrink rapidly. At early times this is possibly the result of increased confinement by the higher molar mass He/O₂ mixture or could simply result from the ablation of less mass. At late times, this is presumably the result of oxidation at the cooler temperatures present at the periphery (see discussion of Fig. 4 below) and as seen in the equilibrium calculations of Hermann and Dutouquet, albeit under a different atmosphere. [20]

State-resolved masses extracted from the images (n.b.- summed over the entirety of each image and thus, no longer spatially resolved) were used to construct Boltzmann plots. Fig. 2 gives representative titanium and vanadium plots under helium. The plots were notably linear, with adjusted R^2 values $>\!0.99$ when at least three points were available. The temperature error bars in Fig. 3 are propagated from the standard error in the slope rather than from replicate Boltzmann plots and do not take into account uncertainties in the reported oscillator strengths.

In considering subsequent Boltzmann-plot analyses of the plasma

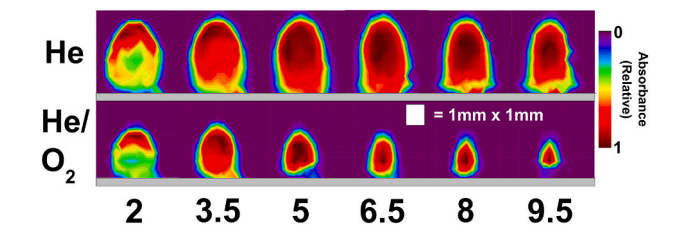


Fig. 1. Titanium ground-term absorption (525.2099 nm absorption line) maps at delays (μ s) indicated below images. Note that images are individually color-scaled to emphasize morphology in comparisons. Note also that the spatial axes are not isometric.

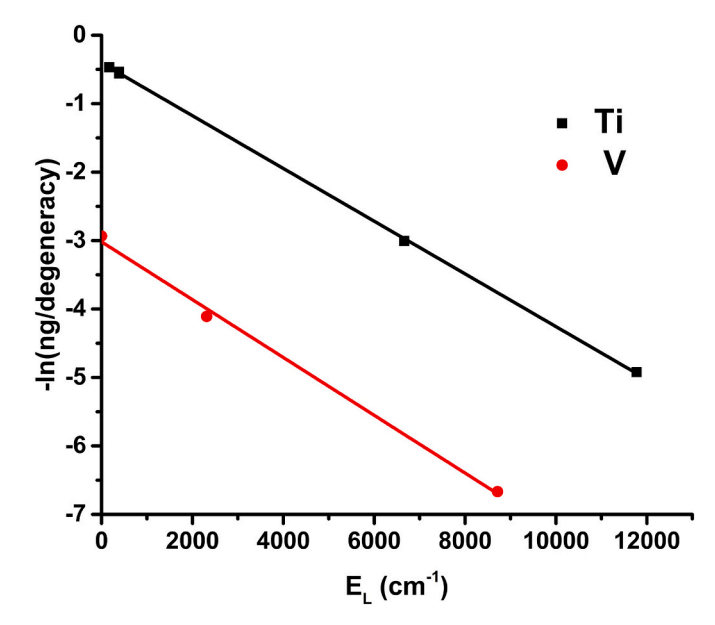


Fig. 2. Representative Boltzmann plots under helium cover gas at delay of 5 μ s. The masses used for the y-axis are summed over the entire plasma image and do not represent any single region of the plasma.

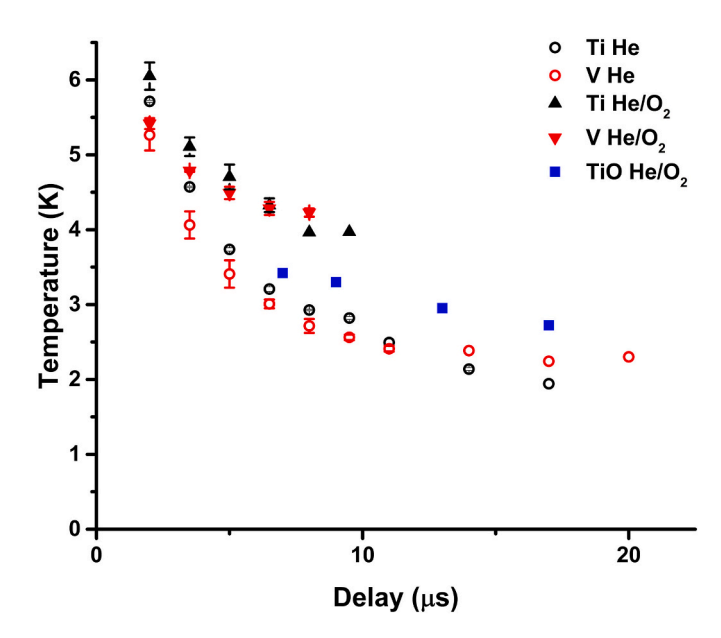


Fig. 3. Electronic excitation temperatures of titanium and vanadium neutrals under different cover gases. Temperatures calculated from absorption summed across entire plasma image. Error bars reflect the error propagated from the standard error in the slope (when available). See text for interpretation of TiO (rovibrational) temperatures.

maps, it must be remembered that the relative populations are measured here in absorption of the ground term or of relatively low-lying metastable levels (see Table 1) whose transitions to the ground state are parity-forbidden. Furthermore, the present measurements are summed across the entire plasma. This is in contrast to the thermal emission measurements from relatively higher-lying energy levels with vague representation across plasma morphology and mass typically found in the literature. These different diagnostic techniques can result in differing perspectives on the plasma. For example, LaHaye et alia's neutral excitation temperatures (measured in emission) were higher than neutral Doppler temperatures (measured in absorption) but were in agreement with first-ion kinetic Doppler temperatures measured in

absorption. [9] Presumably, this is because each measurement represents a distinct region of the plasma.

Fig. 3 indicates that at delays of 5 µs and beyond, the vanadium and titanium excitation temperatures were grossly identical. A plateau at ~2300 K is apparent in the measurements with a pure He atmosphere. This is notably less than the pressure-adjusted boiling point of either metal but might be rationalized by the degree of mixing with the background gas (i.e. because of reduced partial pressure). There was insufficient signal-to-background ratio under He/O2 to generate the necessary absorption maps at long delays, but the atomic temperatures under the oxidizing atmosphere are significantly higher than those under pure He at all times measured beyond 3.5 μ s. Whether this is because of differences in thermal conductivity and/or mixing or the result of heating by the exothermic metal-oxygen bond formation is unclear. We do note that Harilal et al. found that increasing oxygen partial pressures in an argon/oxygen mixture led to faster decreases in uranium excitation temperatures measured with emission spectroscopy at a total pressure of 100 Torr. [19] In their case, however, the oxygen has the opposite relative effect on thermal conductivity.

The excitation temperatures above approximate the plasma as thermodynamically homogeneous. In order to investigate the gradients, lateral scans of the titanium absorption were performed at a single height (1.4 mm) and delay (5 µs) under pure He (see Fig. 1 for location in the plasma at this delay). The 546.050 nm titanium line was scanned seven times with the spectrograph operated in slightly increased dispersion (grating double passing with adjacent pixel binning). To compensate for the decreased SNR, the number of shots/line-of-sight was doubled for the double-pass measurements (i.e. 30 vs. 15 ablations). Peaks were fit to a Voigt model with OriginPro 9.1, with Doppler temperatures calculated from the Gaussian components. Fitting neglected the isotope splitting and hyperfine structure. In order to verify that this omission had negligible impact on the calculated Doppler data, a synthetic spectrum was constructed including Gaussian peaks corresponding to each of the even isotopes at their appropriate shifts. Because shifts and splittings of the odd isotopes are not available to our knowledge, these were neglected but should have less effect than the larger 46 Ti and 50 Ti shifts (both $\sim 0.025~\text{cm}^{-1}$ relative to 48 Ti per Reference [27]) considered here. Fits of the synthetic peak sums were only \sim 3% higher than fits of a single (unsplit) Gaussian peak, indicating that neglection of the isotope shifts (and likely the less-shifted but hyperfine structured odd isotopes) did not result in significant error. However, the modest SNR in the experimental data did lead to substantial variation in fits, so each line-of-sight measurement was repeated a total of seven times. Excitation temperatures were also measured via line-of-sight scans with each of the lower state energies. Fig. 4 gives the two temperatures and line-of-sight integrated ground-term peak area at each lateral position. Note that these are presented as raw line-of-sight data; an inverse Abel transformation was not performed since the Doppler measurements would require a wavelength-by-wavelength Abel inversion, which would require an extremely high SNR.

The line-of-sight-resolved Doppler and excitation temperatures are equivalent and show the expected gradient, with higher temperatures observed when probing lines of sight through the plasma center. The full-plasma-integrated excitation temperature under these conditions is 3700 K, only slightly lower than the temperature measured near the center of the scan. While we have not characterized the random error in the scanned excitation temperatures, the extremely smooth trend (neglecting the point at the far left) suggests that such random error is minor. The data indicate that the electronic and translational degrees of freedom are in mutual equilibrium at these late delays such that Doppler measurements may be used to approximate the excitation temperature. Note that these Doppler data do not include highly excited levels, but rather represent the environment dominated by the lower-energy levels most relevant to understanding the disposition of cooling plasma mass at these long delays.

Knowledge of the temperature (and therefore the partition function)

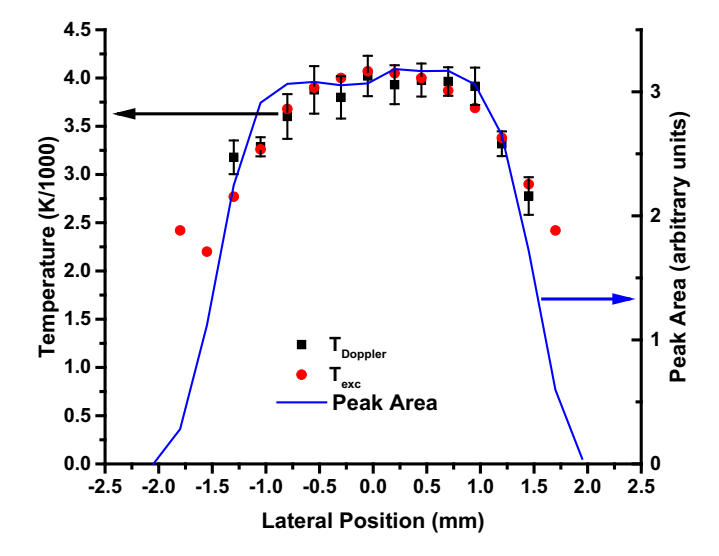


Fig. 4. Lateral scan of titanium Doppler and excitation temperatures 1.4 mm above sample surface. Error bars on Doppler temperatures are one standard error (n=7). Measurements performed under helium at 5 μ s. The ground term's absorption peak area is also graphed (solid line) to provide a spatial reference to the temperature data.

and the absolute population of any one level in the atomic state distribution function allows estimation of the total neutral mass of the plasma with Eq. (2). The extracted masses of vanadium and titanium are given in Fig. 5. The uncertainties (when present) are propagated from the respective standard errors in the calculated slope and intercept. Their propagation as uncorrelated, which is not strictly correct, may under or overestimate the uncertainties. As such, uncertainties are provided as a rough estimate. However, by measuring at or near the ground level (which is substantially more populated at these later times), the uncertainties in total mass are reduced substantially. This is in contrast with the case where only excited states are probed and substantial extrapolation back to the ground state is required, as in calibration-free LIBS.

The plots show the expected ingrowth of neutral population at early times as electrons and ions recombine. The source of the dip in apparent

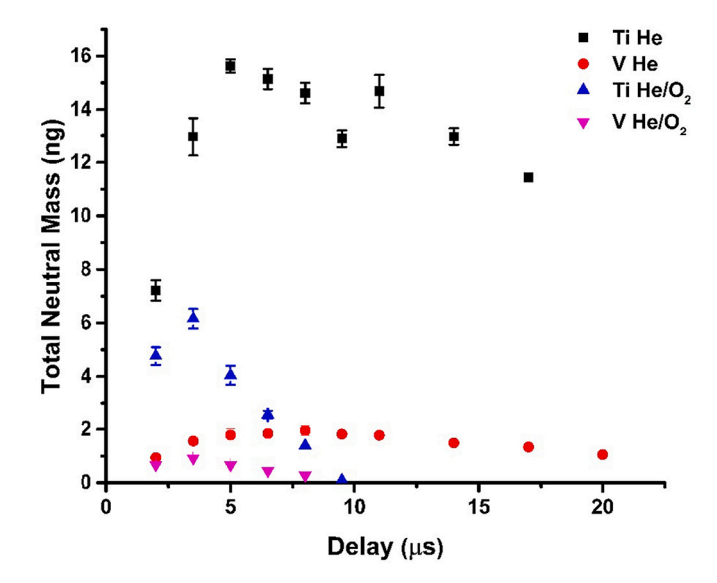


Fig. 5. Evolution of total (plasma-integrated) neutral vanadium and titanium masses calculated using Boltzmann plots and Eq. (2). Error bars, when present, are propagated uncertainties from the standard errors of slope and intercept of the Boltzmann plots.

titanium population at 10 us under helium is unclear but has been found to be reproducible. Under pure helium, both the titanium and vanadium data show a modest loss of measured atomic material at long times (beyond 8 µs). This could be due to reaction with residual oxygen in the chamber and/or formation of metallic diatomics, or deposition onto surfaces (i.e. bulk sample or particles and droplets). The boiling point of titanium at this pressure is \sim 3300 K, lower than the measured excitation temperature under pure helium beyond 5 µs. Local partial pressures are likely to be substantially <300 mbar, permitting further cooling without condensation (or invoking supercooling). Nonetheless, the discrepancy is sufficient to suggest some error. It is also possible that the electronic excitation and kinetic temperatures are not in equilibrium at these late times (and that the kinetic temperature is higher), however the data in Fig. 4 do not support such a claim. Note that all of the data are spatially averaged (either simple line-of-sight or multiple line-of-sight), which further complicates conclusions. For example, the higher temperatures observed under He:O₂ might be the result of the consumption of atoms in the cooler spatial regions of the plasma by chemical reactions, leaving these plasmas to be represented in our atomic absorption data by the hotter (and thus, unreacted) regions of the plasma.

In order to better understand the route of loss of material at these long times, we complement our atomic absorption measurements with TiO A-X $\Delta \nu = 0$ emission spectra. The plasma was imaged with $\sim 1.5 \times$ demagnification onto a round-to-linear fiber optic bundle coupled into a Czerny-Turner spectrograph (f = 0.5 m, 1200/mm grating) employing ICCD detection (Andor iStar) with a gate width of 2 µs. These optics result in a somewhat ambiguous spatial representation of the plasma. The emission at identical delays (8 µs) under the two atmospheres is given in Fig. 6. There is no discernible TiO emission under helium, including measurements integrating from 8 to 16 µs (not shown), suggesting that residual oxygen and leaks are insignificant under the pure He atmosphere, though the comparison is complicated by the different temperature profiles under the two atmospheres- i.e. the lower temperature under He may decrease sensitivity of the emission measurement. Furthermore, given that these measurements are made with a static atmosphere, the extent of infiltrating or residual air concentration may not be entirely reproducible.

In the long term, we are interested in using these absolute measurements to understand plasma stoichiometry. In turn, this requires understanding of the dynamics and full disposition (neutral atom, ion,

molecules, etc.) of the ablated mass. Our setup is not appropriate for measuring entire molecular bands in absorption, nor can it measure transitions with wavelengths below 405 nm at present, preventing analogous measurements of ions. These limitations preclude more specific conclusions about the measured maxima in the measured neutral mass. Strictly speaking, the maxima in Fig. 5 only indicate equality of the rates of loss and creation of neutral gas-phase atoms (averaged across all processes and across the entire plume). For example, arbitrarily assuming that electron-ion recombination is the only source of the increase in atomic population before \sim 8 μ s and that sinks of atomic population are negligible, we find that both the titanium and the vanadium in the plasma remain 50% ionized at 2 μ s under pure He. Given that the observed maximum in the neutral Ti population may underestimate the true extent of atomized material before 8 μ s, we should consider this a lower bound on the ionization fraction at 2 μ s.

Considering the clear appearance of molecular peaks in the absorption spectra under He/O2 (data not shown) and the emission spectrum of Fig. 6, interpretation of the persistence curves in Fig. 5 requires consideration of the formation of TiO, VO and higher metallic oxides, possibly even concurrent with the recombination that dominates the first few microseconds of plasma evolution. The maximum neutral masses under the oxidizing atmosphere are clearly lower by a factor of two for both metals and are shifted earlier in the plasma's development (i.e. 3.5 under He/O₂ vs. \sim 8 µs under He), despite the higher temperatures observed under He/O2. This lower maximum could be because of decreased initial material removal and atomization, perhaps because of the rapid formation of an oxide surface layer on the sample between laser shots. Alternatively, the decreased peak value could be due to rapid loss of atomized material to oxidation post-ablation (i.e. concurrent with recombination), despite having removed a mass similar to that removed under the noble-gas atmosphere. Without access to information on the ion population at early delays when the relative importance of oxidation is presumably less and when the plasma is highly ionized, it is not possible to rule out either possibility.

Although it is theoretically possible to use our setup to measure molecular spectra in absorption, our limited simultaneous observation range makes such an experiment unreasonable, unlike the dual-comb technique used by Jones' lab. [23] As a result, we are left to study oxide formation either by emission (when possible), or indirectly, by measuring the disappearance of the atomic population. Fig. 7 shows the

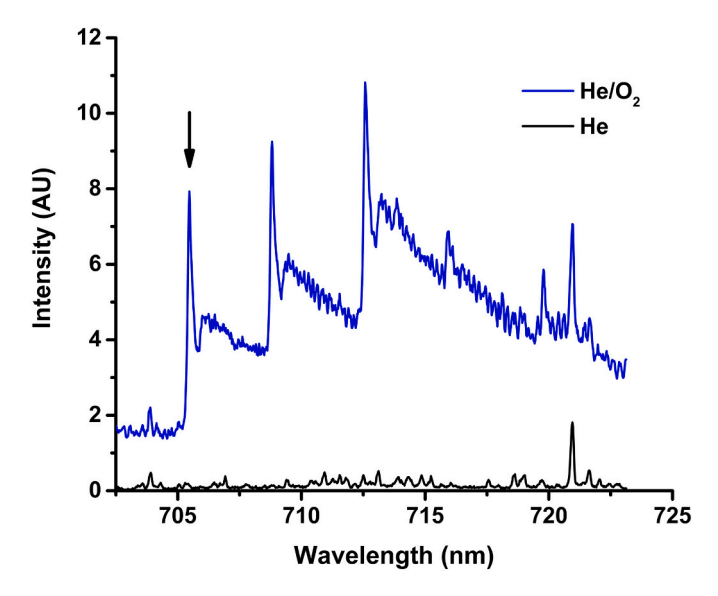


Fig. 6. Vicinity of TiO A-X $\Delta \nu=0$ band measured in <u>emission</u> under He and He/O₂ atmospheres with 2 μ s gate centered at 9 μ s. The arrow indicates the feature used for Fig. 7. Rovibrational temperatures extracted from the molecular emission spectra are included in Fig. 3.

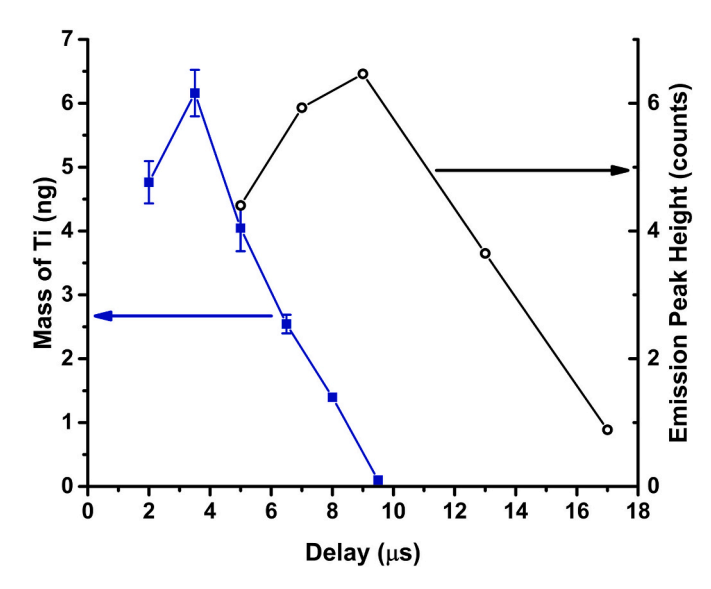


Fig. 7. TiO emission bandhead height and Ti neutral mass (from Fig. 5) as function of delay. The spectral feature selected for the emission measurement is indicated with the arrow in Fig. 6. Error bars on the Ti mass data are propagated from the standard errors in the Boltzmann plot.

evolution of the vapor-phase neutral titanium mass (measured in absorption) under He/O₂ plotted with the *emission* signal from the ~705nm TiO emission feature indicated in Fig. 6. Fits of the molecular spectra using the software available in Reference [28] yielded the rovibrational temperatures included in Fig. 3. These molecular temperatures are notably lower than the neutral atomic excitation temperatures under the same cover gas- in fact, they are more similar to the excitation temperatures under pure helium. This observation supports our suggestion that the higher temperatures measured under He:O2 result from the selective loss of the coolest spatial portions of the plasma to chemical reaction, with the plasma subsequently represented (in the atomic absorption-derived temperatures) by the hottest regions of the plasma. The TiO emission persists ${\sim}9~\mu s$ beyond the neutral atomic mass in the plasma. Given that, under the oxidizing atmosphere, there is no further atomized mass available to form TiO beyond 9.5 µs, the losses in TiO emission signal after this point (i.e. the TiO emission maximum) are presumably due to a combination of a) the observed decrease in temperature (see rovibrational data in Fig. 3) to populate the excited molecular electronic state, b) loss of TiO to formation of higher oxides and deposition as particles and c) diffusion out of the area of observation.

The mass persistence curves in Fig. 5 allow some insights into the stoichiometry of the neutral populations, which may or may not be applicable to the total atomized (i.e. neutral + ion) populations. Fig. 8 plots the ratio of the neutral atomic populations for the two metals as a function of delay. Under helium the ratio is constant and matches the nominal alloy composition. At early times (when ionization is expected to be high), this is partly due to the minimal difference in ionization energies of the two metals (Ti = 6.828 eV, V = 6.746 eV) [29], with the difference partially offset by the ratios of partition functions. [26] Under He/O₂, the ratio is grossly consistent with the nominal sample stoichiometry at 2 μ s but becomes increasingly enriched in atomic vanadium as delay increases.

With the assumption of LTE, the ratio of any given element's (A) atom number density to its first oxide (AO) as a function of temperature follows:

$$\frac{n_A n_O}{n_{AO}} = \frac{\left(2\pi\mu kT\right)^{3/2}}{h^3} \bullet \frac{Q_A Q_O}{Q_{AO}} \bullet e^{\left(-\frac{D_0}{kT}\right)}$$
(3)

where n is the number density of the indicated species, μ is the reduced

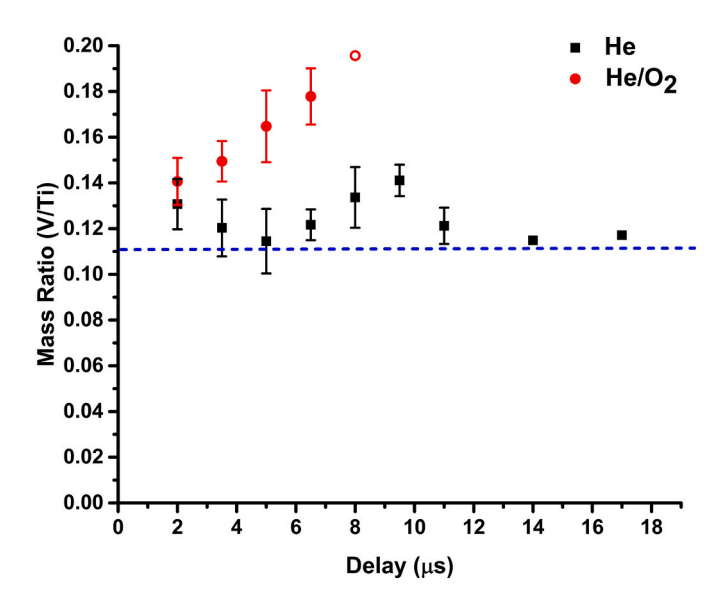


Fig. 8. Stoichiometric ratio of absolute neutral masses in plasma. Masses are taken from Fig. 5- i.e. extracted from whole-plasma Boltzmann plots generated from absorption measurements. Error bars (when shown) are propagated from the uncertainties in the respective masses.

mass of the A + O collision pair, T is the temperature, h is Planck's constant, k is Boltzmann's constant, Q is the partition function of the indicated species, and D_o is the metal oxide's dissociation energy $(D_0(TiO)=6.87~eV,~D_0(VO)=6.545~eV)$. [30,31] Because there are more reactant particles than product particles, the mass densities would required for calculations for a single metal-oxide system with the present measured masses. However, applying Eq. (3) to each of the two metal-oxide systems and ratioing the equations gives:

$$\frac{\left(\frac{n_V}{n_{VO}}\right)}{\left(\frac{n_{Ti}}{n_{TiO}}\right)} = \frac{\left(\mu_{V-O}\right)^{3/2}}{\left(\mu_{Ti-O}\right)^{3/2}} \bullet \frac{Q_V Q_{TiO}}{Q_{Ti} Q_{VO}} \bullet e^{\left(\frac{D_{0,TiO} - D_{0,VO}}{kT}\right)}$$

$$\tag{4}$$

Applying the bond energies from References [30,31] and partition functions from References [32,33], we plot the expected ratio of atom: oxide ratios (i.e. Eq. (4)) as a function of temperature in Fig. 9. Assuming thermodynamic equilibrium and neglecting chemistry beyond the formation of the first oxide, we thus expect the plasma to become (relatively) enriched in V atoms as it cools under He/O2. This interpretation ignores the contribution of the ion-atom equilibria to the elements' neutral extent at the higher temperatures, though this contribution should be slight given that the difference in titanium and vanadium's first ionization energies is <0.1 eV and that the degree of ionization is likely modest by 3.5 µs. In contrast, if we assume that the declines in neutral atomized mass (Fig. 5) at long delays are due to formation of VO and TiO (despite the absence of detectable molecular emission spectra), this is clearly significant beyond 3.5 µs and possibly before, particularly if we assume that the difference in maximum atomized mass between the He and He/O2 atmospheres is due solely to oxidation after ablation of otherwise equivalent masses of metal. Once again, measurements of ionized mass at early times would allow a more complete understanding of the importance of gas-phase oxidation (and other chemistry) on the observed maxima in the atom masses.

The data in Fig. 5 show a modest loss of atomized metal at late delays even with the pure helium atmosphere. However, the Ti/V ratio is approximately constant under the noble atmosphere, even at longer delays. Assuming that there are no sources of additional mass at long delays, there must be a mechanism for material loss at long times that is independent of the analyte (i.e. not selective), in contrast to the element-dependent oxidation behavior. This suggests against substantial reaction with residual oxygen in the chamber to form TiO at the conditions and times used here. The bond dissociation energies (D_0) for Ti_2 and V_2 are

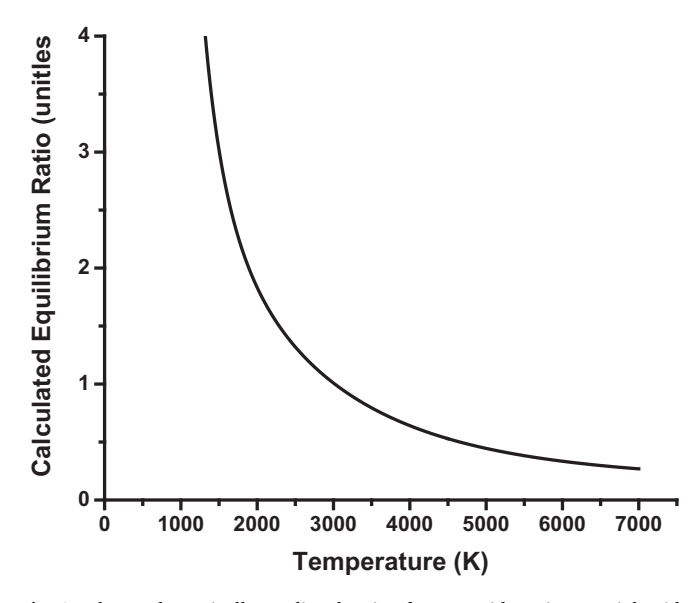


Fig. 9. Thermodynamically predicted ratio of atom/oxide ratios per right side of Eq. (4). References for thermodynamic quantities are given in the text.

fairly distinct (1.4 and 2.8 eV) [34] and would lead to enrichment in titanium as the plasma cools (ignoring potential differences in molecular partition functions) if there were substantial formation of these diatomics. Spain and Morse report the TiV heteronuclear diatomic as having an intermediate dissociation energy of 2.1 eV. [35] Any substantial TiV formation would also lead to relative enrichment in Ti given its abundance relative to V. The absence of titanium enrichment under He at late delays suggests that either such metal diatomic formation is not the main mechanism of loss or it is compensated by another mechanism effecting an opposite enrichment. However, given that the loss is slight within the delays measured, a substantially selective mechanism would be required to create observable fractionation under the He atmosphere. Vanadium and titanium do have nearly equal molar masses, so diffusion out of the field of view (and below the measurement noise threshold) could account for the slight decrease since it would not lead to fractionation. We should also note that (for the sake of simplicity), this discussion neglects the potential contributions of iron and aluminum, the minor alloy constituents.

4. Conclusions

Atomic absorption spectroscopy has been used to follow the evolution of neutral titanium and vanadium absolute masses in a laser-induced plasma. Because the technique can directly probe the ground-term states dominant in the atomic state distribution function in cooled plasmas, the uncertainties in the measured mass ratios should be lower than those taken from atomic emission Boltzmann plots (i.e. CF-LIBS) requiring extrapolation to the ground state. Of course, there is unavoidable potential for determinate error resulting from the tabulated oscillator strengths, which may be systematic in some situations, e.g. as discussed in Weeks et al.'s recent work on gadolinium oscillator strengths [36].

Even with potential systematic error in the oscillator strengths, the temporal trends in our data and the comparison between the two atmospheres provide clear evidence of post-ablation fractionation in the neutral atomic population by 3.5 µs, potentially due to differential oxidation equilibria (only the first oxidation was considered here). Accounting for this chemistry when using laser ablation as an analytical technique requires attention to the chemical environment of the plasma as controlled by the sample and standard stoichiometry (e.g. the presence of oxides in the sample) and the cover gas makeup (e.g. air vs. noble gas). Although not explored here, the potential impact of the sample oxygen content on the plasma's dynamic chemistry recalls the importance of matrix-matching, a difficult issue if LA-based analytical methods are to avoid sample preparation. It should be noted that our comparison of He to a convenient He/O2 mixture (rather than air) likely exacerbates the apparent impact of post-ablation bond-formation equilibria because of helium's high thermal conductivity and the consequent rapid cooling.

Because our lab intends to use LA-AAS to measure total ablated masses in laser ablation plasmas, we need to understand the dynamics of the various reservoirs of ablated material. Surveying the all of the potential reservoirs for ablated material (atoms, ions, molecules, etc.) for material is experimentally unreasonable. In an attempt to simplify the measurement, we will focus on the combined neutral atomic and (atomic) ion populations of yttrium in a future publication. Specifically, we hope to use such combined measurements to better understand the loss of neutral mass observed at late times in the current work.

In the present experiments, we avoided the lowest-concentration sample components (Fe and Al) because measuring their less-populated excited states requires the use of strong transitions that are likely to saturate with our pulsed probe laser. Given the agreement between the measured titanium and vanadium temperatures measured here it may be appropriate to extrapolate these to the minor elements (particularly at times beyond 5 μs where the agreement between Ti and V temperatures was best). Because of the relative insensitivity of our

method of measuring total mass to uncertainties in the temperature (i.e. through the partition function), we will combine masses found in minor element ground-term levels with major-element-derived temperatures to quantitate the minor elements with minimal error.

Author statement

Jonathan Merten- funding, experiment design, data processing, manuscript preparation.

Erin Nicholas- data collection and processing.
Shawnda Ethridge- data collection and processing.
Hannah Bariola- data collection and processing.
Shealyn Chestnut- data collection and processing.
Anna Anders- data collection and processing, experiment design.
Jackie Brees- data collection and processing.
Mary Foster- data collection and processing.

Declaration of Competing Interest

None.

Data availability

Data will be made available on request.

Acknowledgements

This work was supported by NSF award number 1905301. The authors thank J. Hermann, S. Harilal, W. Burns and H. Koizumi for helpful conversations.

References

- J. Lawrence, Advances in laser materials processing, in: Welding and Other Joining Technologies, Woodhead, Duxford, United Kingdom, 2018, p. 779.
- [2] J.P. Singh, S.N. Thakur, Laser-Induced Breakdown Spectroscopy, Elsevier, Amsterdam, 2007, p. 429.
- [3] A.W. Miziolek, V. Palleschi, I. Schecter, Laser-Induced Breakdown Spectroscopy (LIBS), Cambridge University Press, Cambridge, 2006.
- [4] D.W. Hahn, N. Omenetto, Laser-induced breakdown spectroscopy (LIBS), part II: review of instrumental and methodological approaches to material analysis and applications to different fields, Appl. Spectrosc. 66 (2012) 347–419.
- [5] R.E. Russo, X. Mao, H. Liu, J. Gonzalez, S.S. Mao, Laser ablation in analytical chemistry—a review, Talanta 57 (2002) 425–451.
- [6] D.W. Hahn, N. Omenetto, Laser-induced breakdown spectroscopy (LIBS), Part I: review of basic diagnostics and plasma-particle interactions: still-challenging issues within the analytical plasma community, Appl. Spectrosc. 64 (2010) 335A-366A.
- [7] R.H. Huddlestone, S.L. Leonard, Plasma diagnostic techniques, in: H.S.W. Massey, K.A. Brueckner (Eds.), Pure and Applied Physics, Academic Press, New York, 1965, p. 627.
- [8] J. Merten, Laser-ablation absorption spectroscopy: reviewing an uncommon hyphenation, Spectrochim. Acta B At. Spectrosc. 189 (2022), 106358.
- [9] N.L. LaHaye, S.S. Harilal, M.C. Phillips, Early- and late-time dynamics of laser-produced plasmas by combining emission and absorption spectroscopy, Spectrochim. Acta B At. Spectrosc. 179 (2021), 106096.
- [10] J. Merten, B. Johnson, Massing a laser-induced plasma with atomic absorption spectroscopy, Spectrochim. Acta B At. Spectrosc. 149 (2018) 124–131.
- [11] A. De Giacomo, M. Dell'Aglio, R. Gaudiuso, S. Amoruso, O. De Pascale, Effects of the background environment on formation, evolution and emission spectra of laser-induced plasmas. Spectrochim. Acta B At. Spectrosc. 78 (2012) 1–19.
- [12] Y. Iida, Effects of atmosphere on laser vaporization and excitation processes of solid samples, Spectrochim. Acta B At. Spectrosc. 45 (1990) 1353–1367.
- [13] Q.L. Ma, V. Motto-Ros, W.Q. Lei, M. Boueri, X.S. Bai, L.J. Zheng, H.P. Zeng, J. Yu, Temporal and spatial dynamics of laser-induced aluminum plasma in argon background at atmospheric pressure: interplay with the ambient gas, Spectrochim. Acta B At. Spectrosc. 65 (2010) 896–907.
- [14] X. Bai, F. Cao, V. Motto-Ros, Q. Ma, Y. Chen, J. Yu, Morphology and characteristics of laser-induced aluminum plasma in argon and in air: a comparative study, Spectrochim. Acta B At. Spectrosc. 113 (2015) 158–166.
- [15] N.R. Taylor, M.C. Phillips, Differential laser absorption spectroscopy of uranium in an atmospheric pressure laser-induced plasma, Opt. Lett. 39 (2014) 594–597.
- [16] V.S. Burakov, N.V. Tarasenko, N.A. Savastenko, Plasma chemistry in laser ablation processes, Spectrochim. Acta B At. Spectrosc. 56 (2001) 961–971.

- [17] K.C. Hartig, B.E. Brumfield, M.C. Phillips, S.S. Harilal, Impact of oxygen chemistry on the emission and fluorescence spectroscopy of laser ablation plumes, Spectrochim. Acta B At. Spectrosc. 135 (2017) 54–62.
- [18] E.J. Kautz, P.J. Skrodzki, M. Burger, B.E. Bernacki, I. Jovanovic, M.C. Phillips, S. S. Harilal, Time-resolved imaging of atoms and molecules in laser-produced uranium plasmas, J. Anal. At. Specrom. 34 (2019) 2236–2243.
- [19] S.S. Harilal, E.J. Kautz, B.E. Bernacki, M.C. Phillips, P.J. Skrodzki, M. Burger, I. Jovanovic, Physical conditions for UO formation in laser-produced uranium plumes, Phys. Chem. Chem. Phys. 21 (2019) 16161–16169.
- [20] J. Hermann, C. Dutouquet, Local thermal equilibrium plasma modeling for analyses of gas-phase reactions during reactive-laser ablation, J. Appl. Phys. 91 (2002) 10188–10193.
- [21] E.N. Weerakkody, D.G. Weisz, J. Crowhurst, B. Koroglu, T. Rose, H. Radousky, R. L. Stillwell, J.R. Jeffries, N.G. Glumac, Time-resolved formation of uranium and silicon oxides subsequent to the laser ablation of U₃Si₂, Spectrochim. Acta B At. Spectrosc. 170 (2020), 105925.
- [22] I.B. Gornushkin, V.P. Veiko, Y.Y. Karlagina, A.A. Samokhvalov, D.S. Polyakov, Equilibrium model of titanium laser induced plasma in air with reverse deposition of titanium oxides, Spectrochim. Acta B At. Spectrosc. 193 (2022), 106449.
- [23] R.T. Rhoades, R.R.D. Weeks, S.E. Erickson, C. Lecaplain, S.S. Harilal, M.C. Phillips, R. Jason Jones, Dual-comb absorption spectroscopy of molecular GeO in a laserproduced plasma, Opt. Lett. 47 (2022) 2502–2505.
- [24] A. De Giacomo, J. Hermann, Laser-induced plasma emission: from atomic to molecular spectra, J. Phys. D. Appl. Phys. 50 (2017), 183002.
- [25] R.R.D. Weeks, Y. Zhang, S.S. Harilal, M.C. Phillips, R.J. Jones, Multi-species temperature and number density analysis of a laser-produced plasma using dualcomb spectroscopy, J. Appl. Phys. 131 (2022), 223103.
- [26] A. Kramida, Y. Ralchenko, J. Reader, N.A. Team, NIST Atomic Spectra Database (Version 5.9), National Institute of Standards and Technology, Gaithersburg, MD, 2021.

- [27] E.M. Azaroual, P. Luc, R. Vetter, Isotope shift measurements in titanium I. Zeitschrift für Physik D Atoms, Mol. Clust. 24 (1992) 161–164.
- [28] C.G. Parigger, A.C. Woods, D.M. Surmick, G. Gautam, M.J. Witte, J.O. Hornkohl, Computation of diatomic molecular spectra for selected transitions of aluminum monoxide, cyanide, diatomic carbon, and titanium monoxide, Spectrochim. Acta B At. Spectrosc. 107 (2015) 132–138.
- [29] S.G. Lias, Ionization energy evaluation, in: P.J. Winstrom, W.G. Mallard (Eds.), NIST Chemistry WebBook, NIST Standard Reference Database Number 69, National Institute of Standards and Technology, Gaithersburg, MD, 2022.
- [30] H.-P. Loock, B. Simard, S. Wallin, C. Linton, Ionization potentials and bond energies of TiO, ZrO, NbO and MoO, J. Chem. Phys. 109 (1998) 8980–8992.
- [31] D.M. Merriles, A. Sevy, C. Nielson, M.D. Morse, The bond dissociation energy of VO measured by resonant three-photon ionization spectroscopy, J. Chem. Phys. 153 (2020), 024303.
- [32] L.K. McKemmish, T. Masseron, H.J. Hoeijmakers, V. Pérez-Mesa, S.L. Grimm, S. N. Yurchenko, J. Tennyson, ExoMol molecular line lists XXXIII. The spectrum of titanium oxide, Mon. Not. R. Astron. Soc. 488 (2019) 2836–2854.
- [33] L.K. McKemmish, S.N. Yurchenko, J. Tennyson, ExoMol line lists—XVIII. The High-temperature Spectrum of VO, Monthly Notices of the Royal Astronomical Society 463, 2016, pp. 771–793.
- [34] J.R. Lombardi, B. Davis, Periodic properties of force constants of small transitionmetal and lanthanide clusters, Chem. Rev. 102 (2002) 2431–2460.
- [35] E.M. Spain, M.D. Morse, Bond strengths of transition-metal dimers: titanium-vanadium (TiV), vanadium dimer, titanium-cobalt (TiCo), and vanadium-nickel (VNi), J. Phys. Chem. 96 (1992) 2479–2486.
- [36] R.R.D. Weeks, M.C. Phillips, Y. Zhang, S.S. Harilal, R.J. Jones, Measurement of neutral gadolinium oscillator strengths using dual-comb absorption spectroscopy in laser-produced plasmas, Spectrochim. Acta B At. Spectrosc. 181 (2021), 106199.